ADVANCED BIOLOGY
www.advanced-bio.com

Atherothrombosis-on-Chip: A Site-Specific Microfluidic Model for Thrombus Formation and Drug Discovery

*Fahima Akther, Jun Zhang, Huong D. N. Tran, Hedieh Fallahi, Hossein Adelnia, Hoang-Phuong Phan, Nam-Trung Nguyen, and Hang Thu Ta**

Atherothrombosis, an atherosclerotic plaque disruption condition with superimposed thrombosis, is the underlying cause of cardiovascular episodes. Herein, a unique design is presented to develop a microfluidic site-specific atherothrombosis-on-chip model, providing a universal platform for studying the crosstalk between blood cells and plaque components. The device consists of two interconnected microchannels, namely main and supporting channels: the former mimics the vessel geometry with different stenosis, and the latter introduces plaque components to the circulation simultaneously. The unique design allows the site-specific introduction of plaque components in stenosed channels ranging from 0% to above 50%, resulting in thrombosis, which has not been achieved previously. The device successfully explains the correlation between vessel geometry and thrombus formation phenomenon as well as the influence of shear rate on platelet aggregation, confirming the reliability and the effectiveness of the design. The device exhibits significant sensitivity to aspirin. In therapeutic doses (50×10^{-6} and 100×10^{-6} M), aspirin delays and prevents platelet adhesion, thereby reducing the thrombus area in a dose-dependent manner. Finally, the device is effectively employed in testing the targeted binding of the RGD (arginyl-glycyl-aspartic acid) labeled polymeric nanoparticles on the thrombus, extending the use of the device to examine targeted drug carriers.

1. Introduction

Atherosclerosis (AS) is a multifactorial, multistep chronic inflammatory disease associated with several risk factors, including endothelial dysfunction, disturbed blood flow, genetic predisposition, hypertension, hyperlipidemia, and diabetes.[1–3] Several vascular attributes such as vessel geometry, disturbed blood flow, shear stress, extracellular matrix (ECM) protein, biochemical and hemodynamic factors affect the pathological progression of AS.[2,4–6] The early development of AS plaque is initiated by the accumulation of cholesterol, white blood cells, calcium, smooth muscle cells, and other substances in the inner layer of the artery[7] that progressively stenosed the vessel lumen and disturbs local blood flow.[8] The stronger the degree of stenosis, the greater the magnitude of flow disturbance and the greater the concentration of mural stress.[8] At the advanced stage of AS, the vulnerable plaque ruptures and introduces plaque components to blood circulation. It leads to the aggregation of the activated platelets on the site of the ruptured plaque and develops atherothrombosis (**Figure 1**A), eventually leading to subsequent clinical episodes such as myocardial infarction.[9,10]

Early detection of atherosclerotic plaque is the prerequisite for eliminating the risk associated with this disease and reducing mortality. Existing 2D in vitro and in vivo AS models have several limitations because of the lack of physiological micro-and macro-environment parameters in vitro and inter-species differences in vivo.[11] The microfluidic-based in vitro blood vessel models are used to fill the gap because they could provide a well-controlled physiological microenvironment by integrating a continuous flow and introducing cell-cell, cell-matrix interaction on the chip.[12,13] This technology only needs a small volume of samples and reagents for simplified but parallel testing, reducing the overall time and cost of the experiments.[14–16]

Though AS evolves in multiple stages, there is a growing need to develop microfluidic AS models that can mimic the microenvironment of different disease stages to elucidate the biological mechanism and provide a platform for assessing the efficacy of therapeutic compounds. To date, researchers mainly focused on developing in vitro blood vessel models

F. Akther, J. Zhang, H. D. N. Tran, H. Fallahi, H. Adelnia, H.-P. Phan, N.-T. Nguyen, H. T. Ta
Queensland Micro- and Nanotechnology
Griffith University
Nathan, Queensland 4111, Australia
E-mail: h.ta@griffith.edu.au
F. Akther, H. D. N. Tran, H. Adelnia, H. T. Ta
Australian Institute for Bioengineering and Nanotechnology
University of Queensland
St Lucia, Queensland 4072, Australia
H. T. Ta
School of Environment and Science
Griffith University
Nathan, Queensland 4111, Australia
The ORCID identification number(s) for the author(s) of this article can be found under https://doi.org/10.1002/adbi.202101316.

DOI: 10.1002/adbi.202101316

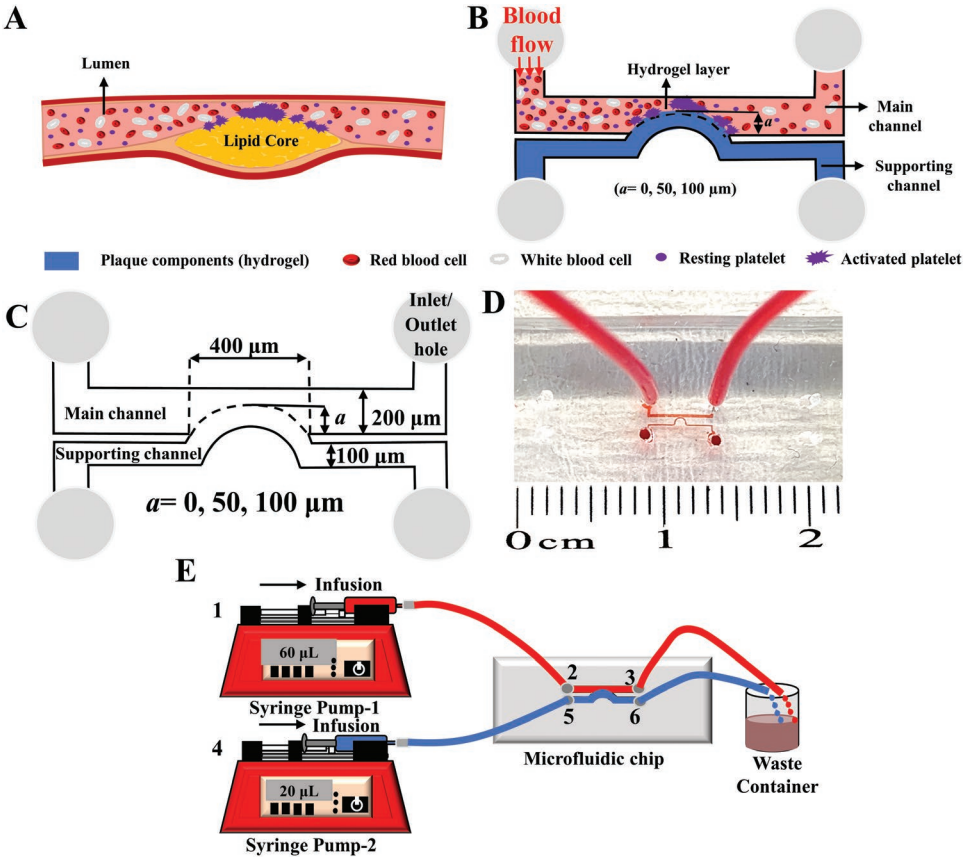

Figure 1. A microfluidic site-specific atherothrombosis-on-chip model. A) Illustration of an atherosclerotic artery with a ruptured plaque, exposing plaque components to the circulation and causing thrombosis. B) Illustration of a proposed in vitro site-specific atherothrombosis model, exposing extracellular components to the circulation and developing thrombosis at that site. C) A schematic diagram of the model. The widths of the main channel and the supporting channel are 200 and 100 µm, respectively. Both channels are interconnected by a 400 µm long porous region. The height of both channels is 50 µm. Each channel has an inlet and an outlet. Devices with different stenosis are fabricated by reducing the width or increasing the blockage height *a* at the porous connecting region. The blockage heights of 0, 50, and 100 µm correspond to 0%, 25%, and 50% stenosis. D) A photograph of the microfluidic atherothrombosis-on-chip device for site-specific atherothrombosis formation. The red dye was used to highlight the microfluidic channels and a ruled was placed to represent the relative size of the device. E) Schematic diagram of the standard infusion process of polymer solution through the supporting channel for obtaining hydrogel scaffold into the supporting channel. 1) The first syringe pump was connected to the inlet 2) of the main channel for infusing phosphate-buffered saline (PBS) (red). 3) A tygon tube was attached to the outlet of the main channel for the waste removal. 4) The second syringe pump was connected to the inlet of the supporting channel 5) for introducing polymer solution (blue) through the supporting channel. 6) A tygon tube was attached to the outlet of the supporting channel for the waste removal.

on-chip, coated with thrombogenic substances such as collagen, and fibrinogen, for studying thrombus formation phenomenon and analyzing drug efficacy. Collagen-coated flow channel is the commonly used system for studying total thrombus formation and quantitative assessment of the antiplatelet and thrombolytic agents at different shear rate.[17–19] Researchers extensively utilized such devices to understand the platelet-derived thrombogenicity and assess drug efficacy using the patients' derived blood samples, including cerebrovascular disease,[20] coronary artery disease,[21] and Kawasaki disease[19] at arterial shear rate. Another typical design for microfluidic devices is the formation of a brief semicircular or an eccentric stenosis region that blocks 20–80% of the channel diameter to generate high shear conditions and observe the resulting clot formation.[22–26] Jain et al.[27] developed a multi-stenosed arteriolar network to monitor the real-time hemostasis and platelet activity. The device could generate shear gradients in the flow, which acts as a hemodynamic activator for clotting. The chip was directly lined up into the porcine vascular access line to prove its reliability as a real-time *ex vivo* diagnostic device. All these previous studies either completely coated the entire device with collagen or inflamed the endothelium throughout the device rather than localizing the thrombotic surface. Furthermore, Yazdani and his colleagues designed a shear-dependent computational thrombus model to study the relationship between shear stress and thrombus formation inclination.[28] The team also studied the influence of shear stress in calculating doses regiment. Meanwhile, bio-printed 3D models developed by Zhang et al.[29] and Costa et al.[30] provided insight into the effect of the vessel geometry and the blood flow pattern in the formation of arterial thrombosis.

To our best knowledge, no study has yet been conducted to mimic the site-specific atherothrombus formation on the chip. According to the literature reviews, all previous designs

used thrombogenic substances to coat the entire channel, and platelets can aggregate across the flow channel. These designs might show a higher aggregation in the stenotic area but could not eliminate the non-specific platelet aggregation in other parts of the flow chamber. Bridging this gap, we designed a novel reusable device with different stenosis that exposed thrombogenic substances in a site-specific manner for focused thrombus formation. The PDMS (polydimethylsiloxane) device consisted of two microchannels, namely main and supporting channels, interconnected by a porous region, named junction region. The supporting channel was loaded with gelatin-collagen composite hydrogel, serving as ECM proteins, and introducing plaque components into the main channel or the flow chamber, simulating the vessel. The novelty of the design is the exposure of the thrombogenic substances to the flow chamber only through the junction region of the two channels that gives a site-specificity. Under in vivo conditions, thrombus formation initiates at the site of plaque rupture (Figure 1A) rather than across the arteries, which is more closely mimicked by our design (Figure 1B). The reliability of the newly developed device was validated in several experiments. We found that the device could successfully explain the influence of vessel geometry and disturb blood flow in thrombus formation propensity. Moreover, the chips exhibited significant sensitivity to antiplatelet therapy. The unique model also provided a robust platform for testing drug carriers for targeted thrombus treatment. Overall, the novel device would deliberate a suitable real-time in vitro platform for tracking disease progression, evaluating effective therapeutic compounds, and modeling targeted carriers for focused treatment.

2. Results

2.1. Designing of Atherothrombosis-on-Chip Model

The novel device consists of two interconnected microchannels: the main channel and the supporting channel. The dimensions of main and supporting channels are 5 mm× 200 µm×50 µm, and 5 mm× 100 µm ×50 µm (length× width× height), respectively. The main channel is used for blood infusion, while plaque-mimicked components (e.g., collagen) are introduced into the circulation by the supporting channel for mimicking the atherosclerotic plaque rupture condition. These two channels are connected via a 400 µm long porous junction region. The size of the pore or the connecting gaps between the two channels is 2 µm. The plaque components are introduced to the circulation through this porous junction. Devices with different stenosis were fabricated by reducing the width of the main channel at the site of the porous junction region by increasing the blockage and mimicking the plaque geometry. The blockage height a is equal to 0, 50, and 100 µm, corresponding to 0%, 25%, and 50% stenosis condition of the main channel, respectively. Each channel has an inlet and an outlet for sample infusion and waste removal. Figure 1C shows a schematic diagram of the microfluidic atherothrombosis-on-chip model and Figure 1D represents a photographic image of the final PDMS microfluidic device. The device is optically accessible for real-time observation with microscope.

2.2. Formation of Hydrogel Scaffold into the Supporting Channel

A 10 wt% gelatin (GEL) solution was initially used to optimize infusion technique to develop the hydrogel scaffold in the supporting channel. Then using the optimized technique (called standard GEL infusion technique), a solution containing gelatin (10 wt%) and collagen (0.02 wt%) (GEL-COL) was introduced into the supporting channel as the plaque components (Figure 1E). The reproducibility of obtaining a relatively homogenous layer of hydrogel over the porous junction region with consistent height was considered for selecting the working protocol.

Using the standard protocol, the pure GEL and GEL-COL solutions were successfully infused through the supporting channel and formed a hydrogel layer over the porous junction region. Because of the hydrogel layer, the total height of the stenosis in the channel changed. After GEL infusion and hydrogel formation, the calculated height of the stenosis peak in the chips with a = 0, 50, and 100 µm was modified to 37.99 ± 1.6, 79.61 ± 2.9, and 130.03 ± 4.35 µm, respectively. Because of the increased blockage height, the corresponding stenosis percentage for the chips with a = 0, 50, and 100 µm were ≈19%, 40%, and 65% (**Figure 2**A). Brightfield images were taken to observe the exposed hydrogel layer over the porous junction region after hydrogel maturation (Figure 2C).

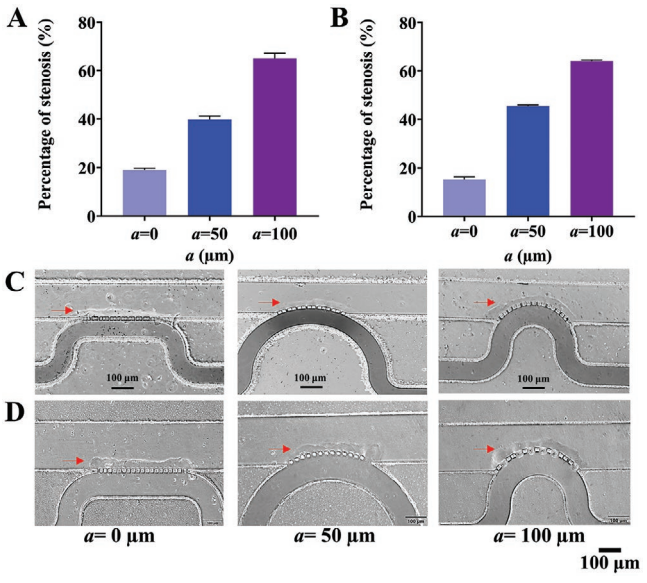

Figure 2. Percentage of stenosis of the chips with different diameter reduction (a = 0, 50, 100 µm) after hydrogel formation over the porous junction region. A,B) Stenosis percentages after forming GEL (10 wt% gelatin) hydrogel, and GEL-COL (10 wt% gelatin+ 0.02 wt% collagen) composite hydrogel, respectively, in the supporting channel (mean ± SD) (n = 3). The height of the stenosis peak changed because of the exposed hydrogel layer over the porous junction area, increasing the overall stenosis percentages in all chips. C,D) Brightfield images of the chips with different blockage heights to observe the exposed GEL hydrogel, and GEL-COL composite hydrogel layer over the junction region in the main channel, respectively. Red arrows indicate the hydrogel layer. The scale bar is 100 µm.

For the devices with GEL-COL composite hydrogel, the height of the stenosis peak varied slightly compared to the chips with GEL hydrogel. The calculated height of the stenosis peak in the chips with a = 0, 50, and 100 µm was modified to 30.50 ± 2.11, 90.91 ± 1.09, and 128.27 ± 0.78 µm, respectively, and the corresponding stenosis percentage was ≈15%, 45%, and 64% (Figure 2B). Brightfield images showed the exposed hydrogel layer over the junction region (Figure 2D). We labeled the chips with the stenosis percentage for the remaining experiments.

2.3. Computational Fluid Dynamics in the 3D Stenosis Geometries

Variations of the shear rate distribution on the curved sidewall in the microchannels with different stenosis were studied numerically using COMSOL Multiphysics 5.6 software. For the 3D construction, only the main channels of the chips with different stenosis were considered because the supporting channels were filled with hydrogel and considered as a solid mesh. Computational fluid flow simulation predicted shear rate distribution on the curved sidewall of the main channel. The base wall shear rate was 1000 s^{-1} for all models presented in this section. The exposed hydrogel layer in the chip with 15% stenosis provided a comparatively flat surface with a slope like structure in the proximal and the distal regions. A rapid rise in the shear rate was observed in the proximal and distal regions of the hydrogel layer (**Figure 3**A) because of the slope formation. However, a small increase in the shear rate at the junction region over the apparently flat hydrogel surface was noticed where the depicted value was ≈1100 s^{-1}. On the other hand, the highest shear rate (γ_{max}) was detected on the apex of the eccentric geometry. The calculated γ_{max} for 45% stenosis and 64% stenosis was 1890 s^{-1} (Figure 3B) and 3450 s^{-1} (Figure 3C), respectively. A 3D simulation was also done to record the shear rates distribution considering all walls in different stenosis and base wall shear rates, presented in supporting materials (Section S5 and Figure S1, Supporting Information).

2.4. Effect of Blood Age on Thrombus Formation

Blood pool time has a significant effect on platelets activity.[31] This study was conducted to investigate the effect of blood age on thrombus formation in the chip. $DiOC_6$ (3,3′-Dihexyloxacarbocyanine Iodide)-labeled blood was infused through the main channel of the 45% stenosed chip containing GEL-COL composite hydrogel in the supporting channel at a base wall shear rate of 1000 s^{-1}. Blood collected within 0–1.5 h showed notable platelet aggregation over time on the GEL-COL composite hydrogel. A significant reduction in platelet aggregation was observed within blood age ranging from 2 to 2.5 h. In comparison, negligible platelet aggregation was noticed with blood older than 3 h (**Figure 4**A). The thrombus entirely covered the curvature radius of the main channel of the 45% stenosed chip after 30 min of perfusion with blood aged 0–1.5 h, while only a layer of platelet was formed over the hydrogel with blood aged 2–2.5 h (Figure 4B). Previous studies supported this observation, as blood was recommended to use immediately or within 2 h of collection.[27,32–35] The effect of blood age was also checked in the device with 15% stenosis, and the results showed a similar pattern (Figure S2, Supporting Information).

2.5. Effect of Channel Stenosis on Thrombus Formation

The percentage of vessel stenosis has a direct influence on thrombosis.[27] Changes in the vessel geometry caused by stenosis create flow disturbance, which in turn initiates platelet adhesion and aggregation.[23] To validate the in vivo relevance

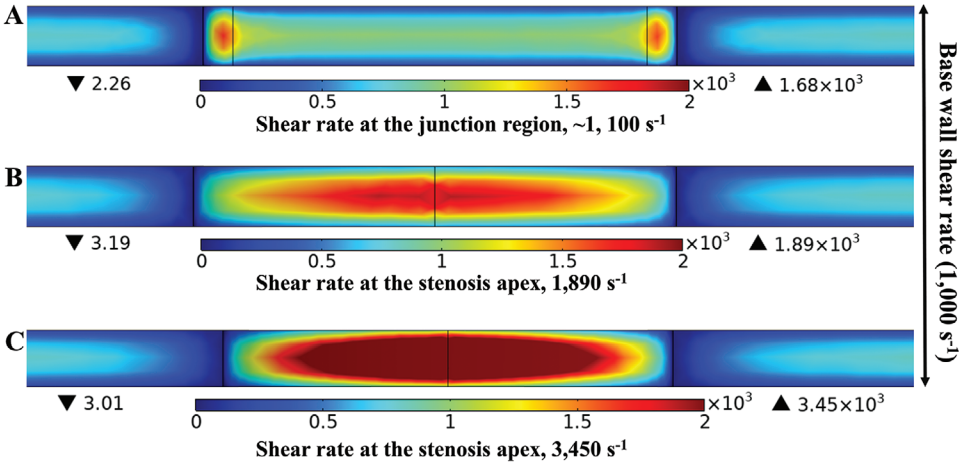

Figure 3. Computational 3D models for calculating the shear rate distribution on the curved sidewall in different stenosis. Computational fluid dynamics analysis displaying the surface shear rate on the curved sidewall in a chip with A) 15%, B) 45%, and C) 64%stenosis. The input base wall shear rate was 1000 s^{-1} in all stenosis. The numerical simulation showed that the shear rate increased at the apex of the eccentric geometry for 45% and 64% stenosis. In comparison, the maximum shear rate was observed in the proximal and distal regions of the chip with 15% stenosis due to the slope formation, while the shear rate at the junction area (over the relatively flat hydrogel surface layer) increased slightly. ** ▲ and ▼ corresponded the highest and lowest shear rate.

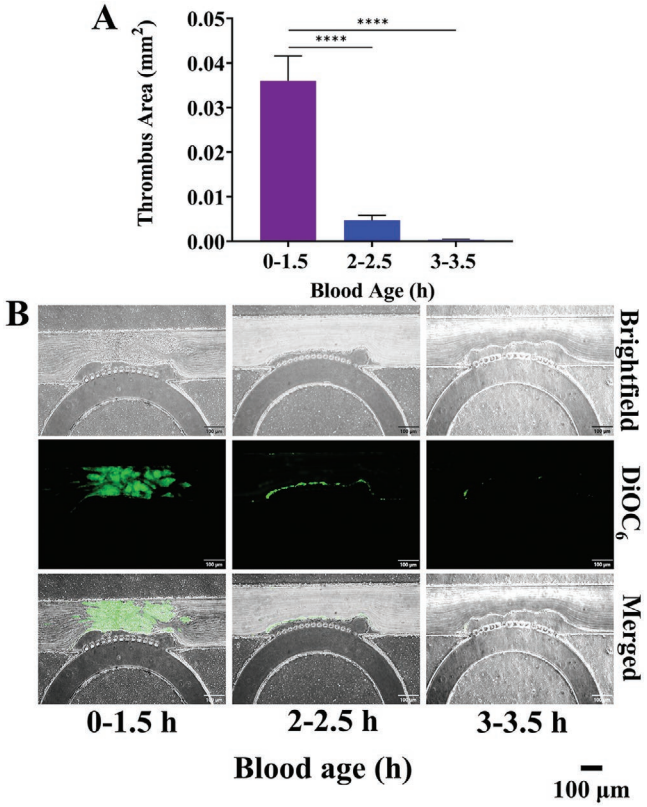

Figure 4. Influence of blood age on the thrombus formation propensity on-chip. Blood was perfused for 30 min through the main channel of the 45% stenosed chip, containing GEL-COL composite hydrogel, at a base wall shear rate of 1000 s^{-1}. Blood age was divided into three windows: 0–1.5, 2–2.5, and 3–3.5 h. A) Comparison of the thrombus area on the 45% stenosed chip with GEL-COL composite hydrogel after 30 min of blood perfusion at a base wall shear rate of 1000 s^{-1} in different time points of blood collection. B) Brightfield, fluorescence, and merged images demonstrated the strong influence of blood age for thrombus formation on the chip. Rapid aggregation of platelet was observed with the blood in 0–1.5 h window and complete blockage of the curvature radius of the main channel was noticed at 30 min. Blood in 2–2.5 h window formed a thin layer of platelet over the hydrogel, while negligible platelet adhesion over the hydrogel was observed in 3–3.5 h window. $^{****}p \leq 0.0001$ compared to the thrombus area by the blood at 0–1.5 h window; $n = 3$; one-way ANOVA test. The scale bar is 100 µm.

of our model, we used chips with different stenosis to investigate the relationship between vessel geometry and thrombus formation phenomenon on the chip. In this experiment, fresh blood within 1.5 h of the collection was used because the blood age influenced the thrombus formation phenomenon, as demonstrated above. $DiOC_6$-labeled blood was infused for 30 min through the main channel of the chip with 15%, 45%, and 64% stenosis containing pure GEL or GEL-COL composite hydrogel at the physiological arterial base wall shear rate of 1000 s^{-1}. There was no platelet aggregation on the chips containing pure GEL hydrogel only (Figure S3, Supporting Information). Chips with GEL-COL composite hydrogel showed a strong correlation between thrombus formation propensity and vessel geometry in a site-specific manner. The first sign of platelet aggregation in the stenosis region was observed within 1 min of blood perfusion. Different stenosed chips were compared by calculating the varying degrees of platelet aggregation over time and thrombus areas.

After perfusing whole blood for 10 min through the devices with 45% and 64% stenosis, a noticeable number of platelets aggregated on the GEL-COL composite hydrogel and the size of the thrombus grew in a time-dependent manner in all devices. Also, a more rapid thrombus growth was noticed in the devices with 64% stenosis when compared to the one with 45% stenosis (**Figure 5**A,B), while only a layer of aggregated platelets was formed over the GEL-COL composite hydrogel on the chips with 15% of stenosis (Figure 5C). The results were consistent with a study from Westein et al [22] where they confirmed the prominent platelet aggregation on the vWF/fibrinogen coated channels with 60–80% reduction, while the single adherent platelet was reported on the chip with 20% stenosis. The recorded thrombus areas for 64% stenosed device in 15 min, 20 min, and 25 min were 0.0163 ± 0.0012, 0.0233 ± 0.0005, and 0.03467 ± 0.0010 mm^2, respectively. On the other hand, the calculated areas for the chip with 45% stenosis were 0.011 ± 0.0027, 0.017 ± 0.0026, and 0.027 ± 0.0027 mm^2 for 15 min, 20 min, and 25 min of blood perfusion successively (Figure 5D). The total occlusion times of the main channel over the stenosis region were ≈20 and 30 min for chips with 64% and 45%, respectively, suggesting a strong relationship between geometry and thrombus formation on the chips (Figure 5E). Occlusion time was mainly determined by the time when the thrombus completely blocked the curvature radius of the main channel. Blockage of the channel with the thrombus did not stop the blood flow entirely but slowed down the flow and started to dislodge the thrombus (Data not shown). The time recorded just before the thrombus dislodgement was considered as occlusion time. No unspecific binding of platelets was observed on the surface of the main channel (Figure S4, Supporting Information).

2.6. Shear-Dependent Platelet Aggregation

An increased shear rate can elevate the internal pressure of the microfluidic channel, reflecting the flow turbulence that causes shear-dependent platelet activation.[18] Microfluidic devices extensively used to study the platelet thrombus formation under different shear rates. Microfluidic flow chamber systems coated with thrombogenic substances showed a proportional increase in thrombus size at different shear rates ranging from 240 to 2000 s^{-1}.[17,18] To validate our device, we investigated the influence of shear rate on platelet aggregation. $DiOC_6$-labeled fresh blood was perfused at the base wall shear rate of 2000, and 3000 s^{-1} into the 15% stenosed device with GEL-COL composite hydrogel. An increase in base wall shear rate resulted in higher shear-induced platelet aggregation. Initial platelet adhesion on GEL-COL hydrogel was similar in both shear rates, but a rapid rise in thrombus area was noticed at the base wall shear rate of 3000 s^{-1} compared to 2000 s^{-1}. Approximately 1.75 times increase in the thrombus area was observed at a base wall shear rate of 3000 s^{-1} compared with 2000 s^{-1} after 15 min of blood perfusion (**Figure 6**A). From the computational 3D models, γ_{max} for both base wall shear rates were noticed at the proximal and the distal regions of the exposed hydrogel due to the slope

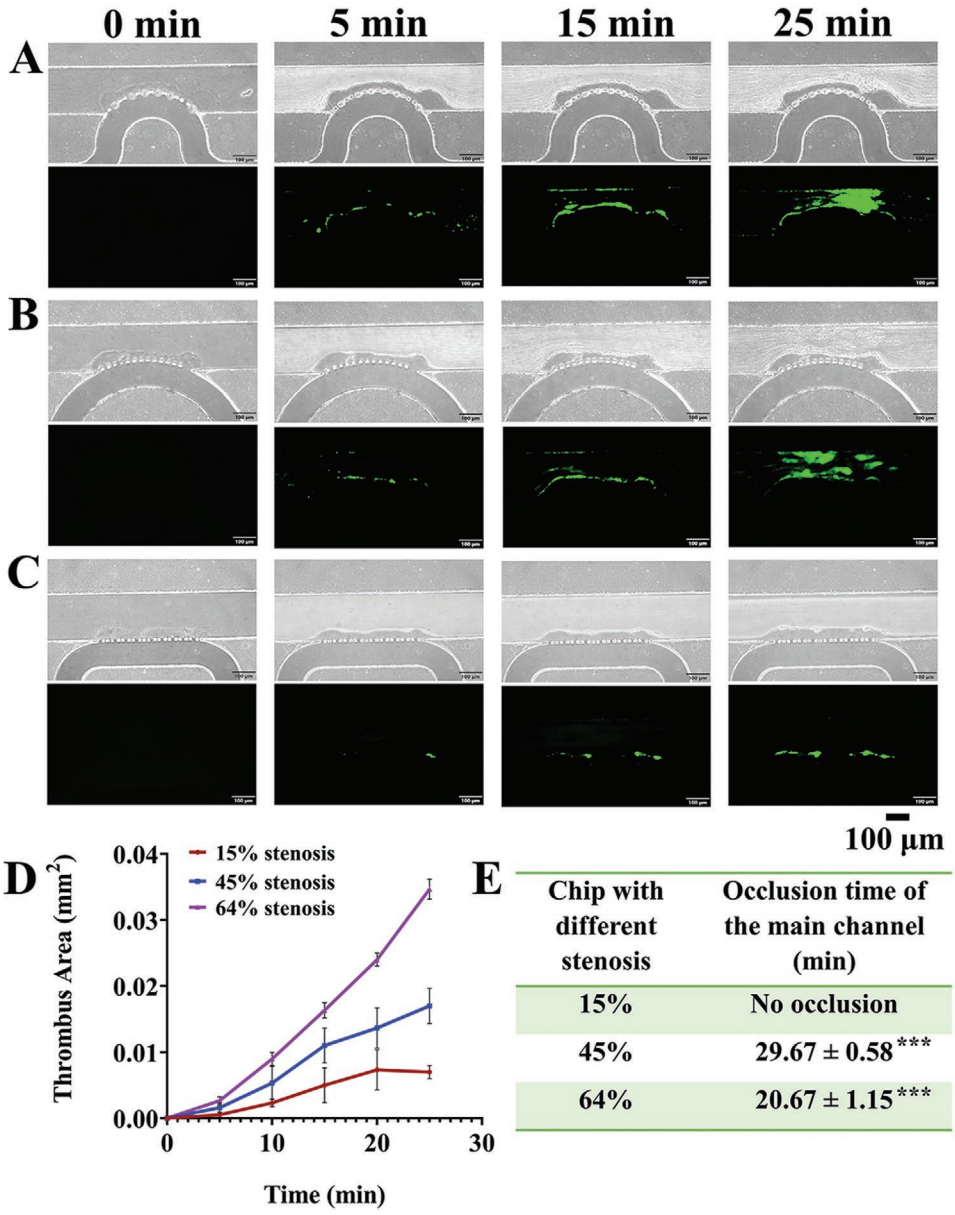

Figure 5. Site-specific atherothrombosis formation on the chip. The blood was perfused for 30 min at a base wall shear rate of 1000 s^{-1}. Brightfield and fluorescence images of the site-specific thrombus formation at the stenosis area of chips with A) 64%, B) 45%, and C) 15% stenosis on the GEL-COL composite hydrogel at different time point. The size of the thrombus increased over time in all chips. D) Comparison of the thrombus area in different time point among different stenosed chips. A rapid growth in the thrombus size was achieved in the chip with 64% stenosis compared to the other stenosis. E) The occlusion time of the main channel at different stenosed chips. No occlusion was observed for the chip with 15% stenosis (***$p \leq 0.0001$ compared to the occlusion time in the chip with 15% stenosis; $n = 3$; one-way ANOVA test). The scale bar is 100 μm.

formation. The recorded γ_{max} for 2000 and 3000 s^{-1} base wall shear rates were ≈3370 and 5070 s^{-1}, respectively. However, the calculated shear rates across the relatively flat hydrogel surface at the junction region were ≈2100 s^{-1} (Figure 6B) and 3250 s^{-1} (Figure 6C) for base wall shear rates of 2000 and 3000 s^{-1}, respectively, indicating a modest increase in the shear rates in that location. Meanwhile, a gradual increase of thrombus area was detected in both base wall shear rates, but no occlusive thrombus was formed after 30 min of blood perfusion (Figure 6D,E).

2.7. Antiplatelet Efficacy of Aspirin on the Chip

Therapeutic concentrations of 50×10^{-6} and 100×10^{-6} M of aspirin were chosen to check the antiplatelet efficacy of aspirin on-chip following the previous studies.[36,37] The size of the thrombus and the occlusion time were evaluated in two different therapeutic concentrations of aspirin (100×10^{-6} and 50×10^{-6} M) in the 64% stenosed chip with GEL-COL composite hydrogel. Aspirin was added in $DiOC_6$-labeled citrated blood and incubated for 10 min before perfusion. Citrated

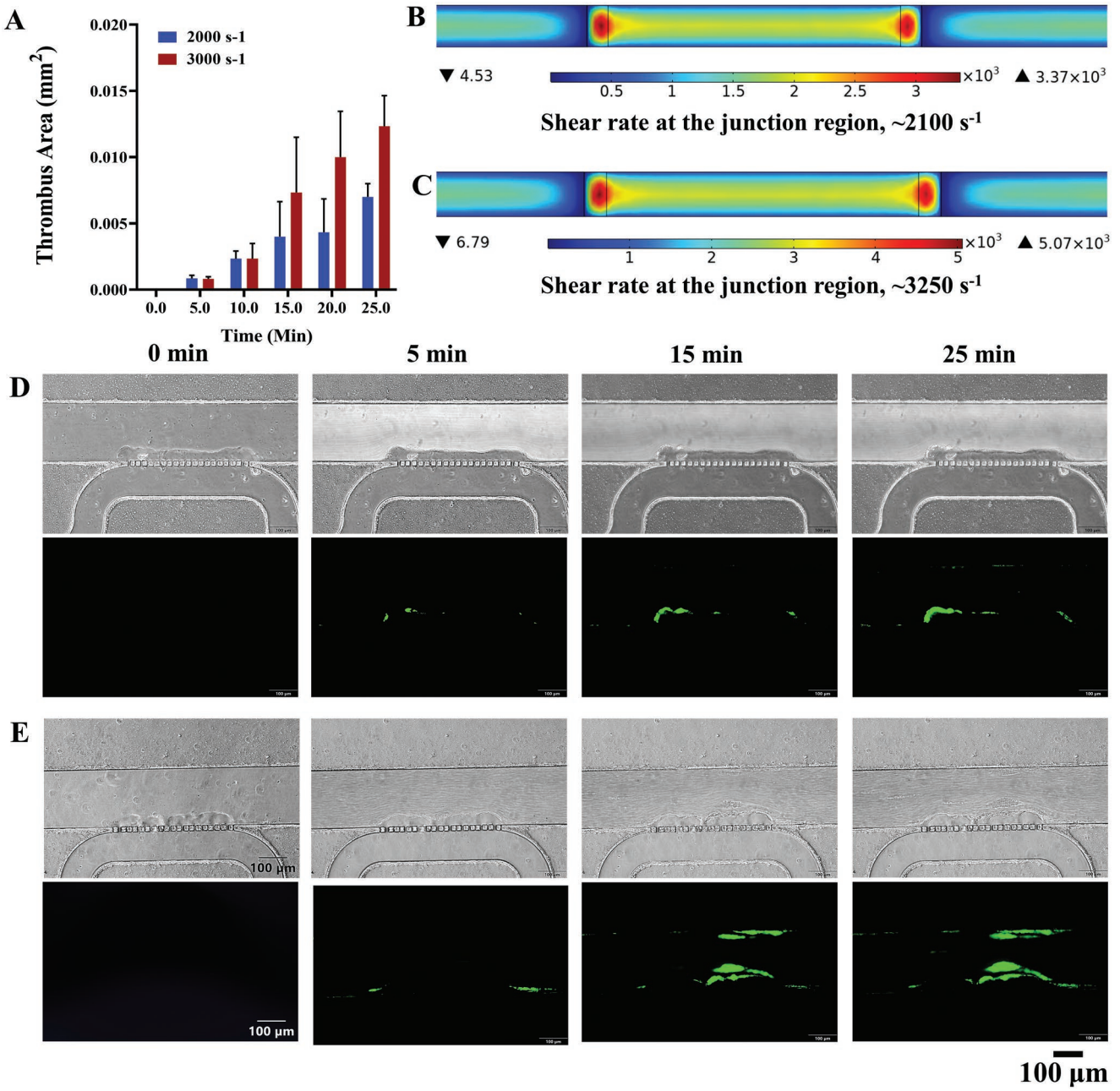

Figure 6. Shear-dependent platelet aggregation in the 15% stenosed chip. A) Calculated thrombus area at different applied base wall shear rates. Computational 3D model for calculating wall shear pattern for input base wall shear rate of B) 2000 s^{-1} and C) 3000 s^{-1} in the main channel. The calculated shear rates on the junction area over the relatively flat hydrogel surface were ≈2100 and 3250 s^{-1} for the base wall shear rate of 2000 and 3000 s^{-1}, respectively. The highest shear rates were recorded in the proximal and distal regions of the hydrogel layer in both cases. Brightfield and fluorescence images of platelet aggregation on the exposed GEL-COL layer at a base wall shear rate of D) 2000 s^{-1} and E) 3000 s^{-1}. A significant increase in platelet aggregation was observed with the increased base wall shear rate. Images of the thrombus area were collected at different time points under the same conditions by perfusing citrated fresh whole blood. The scale bar is 100 µm. ** ▲ and ▼ corresponded the highest and lowest shear rate.

blood is often used to test aspirin effects on platelets and coagulation.[38,39] The chip showed significant sensitivity towards aspirin in a dose-dependent manner. In both therapeutic doses, platelet aggregation on the GEL-COL composite hydrogel reduced remarkably. For 100×10^{-6} M therapy concentration, there was no noticeable platelet adhesion over the GEL-COL composite hydrogel until 20 min. However, very few platelets started to adhere after 15 min of perfusion and formed a thin platelet layer over the hydrogel after 25 min of blood perfusion (**Figure 7**A). For 50×10^{-6} M therapeutic concentration, a slow aggregation of platelets was observed over the GEL-COL composite hydrogel with time, (Figure 7B). The thrombus area in 15 min, 20 min, and 25 min were 0.0033 ± 0.0006, 0.0050 ± 0.0010, and 0.0090 ± 0.0010 mm^2, respectively

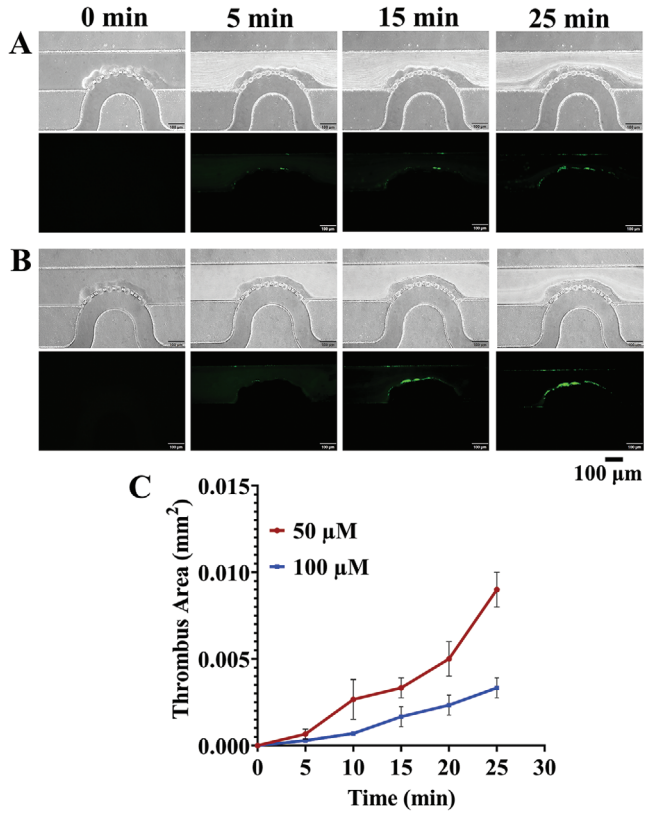

Figure 7. Determination of the antiplatelet efficacy of aspirin on the chip. The blood was infused for 25 min at a base wall shear rate of 1000 s^{-1} in the 64% stenosed chip with GEL-COL composite hydrogel. A) Bright-field and fluorescence image of the site-specific platelet aggregation on the chip with 100×10^{-6} M therapy concentration of aspirin. Very few platelets adhered to the GEL-COL composite hydrogel layer after 15 min of blood perfusion, and a thin layer of aggregated platelets was observed after 25 min of perfusion. B) Bright-field and fluorescence image of the site-specific platelet aggregation on the chip with 50×10^{-6} M therapeutic concentration of aspirin. No occlusive thrombus was noticed over 25 min of blood perfusion. C) Comparison of the thrombus area between the 100×10^{-6} and 50×10^{-6} M therapeutic concentration of aspirin on-chip at different time points ($n = 3$). The scale bar is 100 μm.

(Figure 7C). No occlusive thrombus was observed on the chip within the observation time of 25 min. Overall, both doses remarkably delayed the platelet adhesion and reduced the thrombus area. The results aligned with the previous findings, where 50×10^{-6} M aspirin significantly prolonged the platelet adhesion on the collagen surface[36] while 100×10^{-6} M could prevent the occlusive thrombus formation in arterial base shear rate.[37] This confirms the reliability and accuracy of our newly developed device.

2.8. Targeted Binding of the Arg-Gly-Asp Peptide-Labeled Polymeric Nanoparticles on the Atherothrombosis-on-Chip

The adhesion of Arg-Gly-Asp (RGD) peptide-labeled polymeric nanoparticles (PNPs) to the thrombus was determined in the 64% stenosed device with GEL-COL composite hydrogel as plaque components. 150 nm PNPs were chosen as model vehicles to study the binding of nanomaterials on thrombus. RGD and RAD (Arg-Ala-Asp) peptides were used as platelet-targeting peptides and control non-binding peptides, respectively. The PNPs were also labeled with Cy5 to enable optical fluorescence imaging. The adhesion of the Cy5-RGD-PNPs was observed under base wall shear rate of 1000 s^{-1}. The targeted binding of the PNPs on the thrombus was visible under the fluorescence microscope immediately after the perfusion. The attachment of the Cy5-RGD-PNPs on the targeted thrombus area increased over time (**Figure 8**A). Noticeable binding of Cy5-RGD-PNPs on the thrombus was observed after 2.5 min of perfusion (Figure 8B,C). The targeted PNPs covered the surface of the thrombus completely after 10 min of perfusion and showed strong binding under continuous flow (Figure 8D). On the other hand, Cy5-RAD-PNPs showed insignificant attachment on the thrombus over time (Figure 8E,F) and very few particles bound after 10 min of perfusion (Figure 8G), which indicated that our device could be used as an in vitro physiological relevance platform to evaluate targeting efficiency of drug carrier to treat atherothrombosis.

3. Discussion

AS is a geometrically focused disease associated with chronic inflammation. At the late stage of AS, atherosclerotic plaque ruptures and initiates platelet adhesion and aggregation on the exposed vascular surface, which activates the clotting cascade, leading to the formation of atherothrombus.[40] In this study, we designed and developed a novel microfluidic atherothrombosis model that allows the formation of site-specific thrombus, which has not been achieved previously. The design provides a universal platform to introduce different plaque components in a site-specific manner and develop a focused interaction site for thrombus formation and drug testing. To achieve this aim, we first developed a standard infusion technique using gelatin solution for introducing plaque components. In our device, we used GEL-COL composite hydrogel as simple atherogenic substances and citrated blood (3.2%) without further recalcification to preferentially induce platelet thrombus, also known as white thrombus. Coagulation dominates thrombus formation at low shear rates (e.g., <50 s^{-1}), leading to erythrocyte-rich thrombi that have the appearance of red clots. On the other hand, in arteries, platelet accumulation dominates at higher shear rates, leading to white thrombus formation.[33,41] According to previous studies, when anticoagulated blood is used, the thrombi are formed because of platelet activation only, as the generation of thrombin and fibrin is prevented.[18,42] Collagen type-I is the major ECM protein of human body with a characteristic right-handed triple helical structure and the most thrombogenic component of the sub-endothelium. Resting platelets react with insoluble collagen fibers or an immobilized collagen surface.[43,44] During vascular damage, collagen is exposed to the circulation and triggers both platelets adhesion and activation at the damaged site.[45] The prevailing studies suggested that two receptors are responsible for the platelet responses to the collagen: integrin $\alpha_2\beta_1$ and glycoprotein VI. The integrin $\alpha_2\beta_1$ is responsible for the platelet adhesion to the collagen, allowing platelet to interact with the glycoprotein VI for

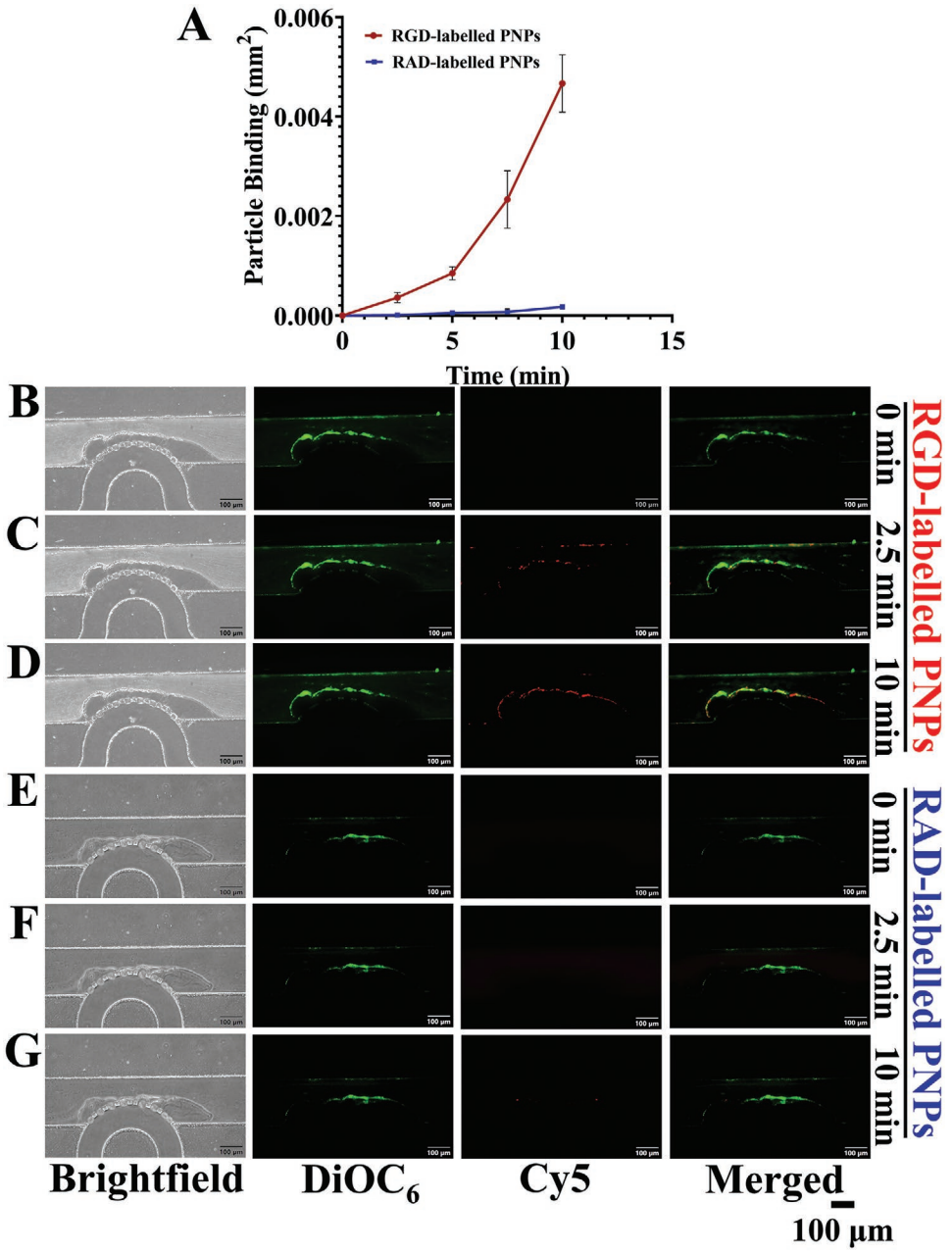

Figure 8. Binding of the targeted (RGD) and nontargeted (RAD) labeled PNPs on the thrombus in the chip. A) Comparison between the targeted and non-targeted PNPs binding affinity on the thrombus at different time point. B–D) Perfusion of the Cy5-RGD-PNPs for observing the binding affinity of the targeted particles at 0, 2.5, and 10 min, respectively. $DiOC_6$ tagged platelets form thrombus (green) on the stenosis area of the 64% stenosed chip with GEL-COL composite hydrogel after 15 min of blood perfusion at a base wall shear rate of 1000 s^{-1}. The binding of the Cy5-RGD-PNPs (red) increased with time and completely covered the surface of the thrombus after 10 min of perfusion. Merged images clearly showed the binding of the nanoparticles on the surface of the thrombus. E–G) Perfusion of Cy5-RAD-PNPs for observing the binding affinity of the nontargeted particles at 0, 2.5, and 10 min, respectively. Insignificant binding of PNPs was observed after 10 min of perfusion ($n = 3$). The scale bar is 100 µm.

platelet activation.[46] Evidences suggested only 5µg mL^{-1} collagen is sufficient to activate the platelets in citrated blood.[47,48] The hydrogel, containing immobilized collagen surface in our system, induced platelet adhesion and activation without any prior recalcification, which was also supported by Westein et al.[22] The team directly used the citrated blood for geometry dependent platelet thrombus formation in a vWF/fibrinogen coated microfluidic chip. In our device, thrombus formation was initiated by the adhesion of the flowing platelets on the thrombogenic surface of GEL-COL composite hydrogel.

The gelatin used in our study is a fibrous protein derived from the thermal denaturation of collagen.[49] Gelatin has the same amino acid sequence as collagen. However, gelatin lacks the triple helical structure of collagen.[50] Such triple helical structures have been reported to be responsible for platelet binding,[51] and thus gelatin alone does not affect

blood coagulation.[52,53] In our device, no platelet aggregation was observed in the device with pure GEL hydrogel. This finding also proved that our design does not promote platelets activation but requires thrombogenic substances-like in vivo conditions. Furthermore, we can easily introduce any thrombogenic substances or complex plaque materials in addition to collagen using the developed standard GEL infusion protocol.

Moreover, our device could mimic the stenosis-dependent-thrombus formation like in vivo conditions. Under a pathophysiological condition, an atherosclerotic plaque grows towards the adventitia until it reaches a critical point, begins to expand outward, and ruptures into the lumen.[54] When the plaque covers more than 40% of the vessel lumen, it is considered occupied.[7] According to the studies, the reported percentage of the stenosis responsible for the coronary occlusion and myocardial infarction is not less than 70%,[55,56] while others suggest over 50%.[57,58] Another study summed up the severity of the disease based on the stenosis grades, where the severity of AS was categorized as mild, moderate, severe, and critical for ≤39%, 40–59%, 60–79%, and ≥ 80% lumen reduction, respectively.[8] The recorded shear rates for the moderate and severe arterial stenosis are 2600–4000 s^{-1}, and >4,000 s^{-1} respectively.[22,59] A possible explanation for such a preferential localization of AS is that the geometry of the vessel affects the blood flow pattern.[3] In our study, numerical results indicated the peak shear rate for the applied base wall shear rate at different stenosis after hydrogel layer formation. The simulated model showed increased peak shear rates for the arterial base wall shear rate (1000 s^{-1}) in both 45% and 64% stenosis, and the corresponding peak shear rates on the apex of the curved sidewall were ≈1890 and 3450 s^{-1}. Furthermore, hemodynamic changes during the constant flow rate experiments because thrombus continually alters the lumen diameter.[60] When blood flow changes from laminar to turbulent/recirculating flow, the flow forms vortices, which significantly increases overall flow resistance.[61] As both flow recirculation and shear rate increase with the severity of stenosis in human coronary arteries,[62] the peak shear rate continuously increases in the stenosis part of our channel with thrombus growth. Increased turbulence might cause rapid activation and attachment of platelets on the wall of the stenosis area that contributes to faster occlusion of the channel. In our study, a device with 15% stenosis did not develop any large thrombus due to a slight increase of shear rate over the relatively flat hydrogel layer at the junction region. A noticeable increase in the thrombus size was detected on the chips with 45% stenosis and 64% stenosis. In addition, occlusion time was significantly lower in the chip with 64% stenosis than in the one with 45% stenosis, which clearly demonstrated the in vivo relevance of our design. Moreover, a previous study also reported the occlusion times of ≈12–17 min for 70–83% stenoses of 1.5 mm test sections at 5000 s^{-1},[60] which also showed a good agreement with our study (≈20 min occlusion time for 64% stenosis).

We also tested the shear-induced platelet aggregation on the chip with 15% stenosis. The shear rate has a profound effect on platelet-surface interaction during arterial thrombosis, and platelet deposition increases with increasing shear rate.[63,64] The increase in shear rate activates platelets and promotes their transport to and around the growing thrombus, leading to increased platelet adhesion and cohesion.[59] We applied base wall shear rate at 2000 and 3000 s^{-1} to achieve the shear rate at ≈1890 s^{-1} (γ_{max} of 45% stenosis) and 3450 s^{-1} (γ_{max} of 64% stenosis) on the exposed hydrogel layer at the junction region, respectively. The calculated shear rates from the computational model were 2100 and 3250 s^{-1} over the relatively flat hydrogel surface for the corresponding base shear rates of 2000 and 3000 s^{-1}. For both models, the maximum shear rates were achieved in the proximal and distal regions of the hydrogel layer. Interestingly, the initial platelet adhesion for both shear rates was also noticed on the distal and proximal areas of the hydrogel, which supported the model accuracy. Significant growth of the thrombus was noticed with increasing shear rate, but the shear increase did not result in the complete occlusion of the channel. Occlusive thrombus formation does not only depend on the shear rate but is also associated with other factors of the vessel geometry such as eccentricity.[59] Flow distribution is also influenced by the stenosis eccentricity, and can cause disrupted blood flow that influences rapid platelet aggregation.[3] The relatively flat hydrogel surface of the device with 15% stenosis may minimise potential recirculation flow than those with 45% and 64% stenosis, causing less platelet aggregation in the similar shear rate increase, resulted in no occlusive thrombus.

Furthermore, we tested the antiplatelet efficacy of a known drug aspirin to evaluate the effectiveness of our chip for drug screening. The formation of the occlusive platelet aggregation on the plaque rupture area often leads to heart attack, and antiplatelet therapy is the mainstay of treatment for atherothrombosis. Aspirin mediates the antiplatelet effects through the irreversible inhibition of platelet-dependent thromboxane A2 formation, a potent vasoconstrictor, and a platelet aggregation inducer.[65] Our chip showed profound sensitivity in evaluating the effect of aspirin at therapeutic relevant doses. In both therapeutic doses (50×10^{-6} and 100×10^{-6} M), aspirin prevented or delayed platelet adhesion and reduced the thrombus area significantly at the base wall shear rate of 1000 s^{-1}. Moreover, our results were consistent with the previous studies.[36,37] Li et al.[36] used a microfluidic device to study the influence of shear stress on antiplatelet therapy. Their results demonstrated that aspirin (100×10^{-6} M) could prevent occlusive thrombosis on-chip at the arterial shear rate. Moreover, Hosokawa et al.[37] used a microchip flow chamber system to quantitatively assess the platelet thrombus formation with or without different antithrombotic agents. Aspirin (50×10^{-6} M) modestly prolonged the platelet aggression on the collagen surface and effectively decreased the area under the flow pressure curve, resulting in unstable platelet thrombus formation.

Microfluidic devices have recently emerged and attracted wide attention in drug screening and personalized medicine.[66] The present work is also relevant to design targeted drug-delivery vehicles for treating atherothrombosis. Targeted drug delivery can reduce dosing and eliminate potential side effects.[67] Besides, nanoparticles (NPs) are getting attention to be employed as a drug carrier because of the smaller size and larger surface area with the customized design for targeted drug delivery.[68] We used RGD labeled PNPs for targeting the thrombus on the chip. RGD peptide can specifically bind to the

platelet on αIIbβ3 receptor.[69,70] The targeted Cy5-RGD-PNPs were specifically bound to the thrombus on the chip, while non-targeted Cy5-RAD-PNPs showed insignificant adhesion. These results extended the use of the device as an in vitro platform for testing and designing targeted drug carriers for focused treatment of atherothrombosis.

AS is a complex multifactorial disorder and any thrombogenic substance can influence both disease initiation and progression.[71] It is crucial to design a simple device that can serve as a versatile platform for investigating the effect of each responsible component on AS development. To our best knowledge, this is the first design that incorporates vessel complexity and plaque components together to develop an in vitro site-specific atherothrombosis-on-chip model. Our atherothrombosis-on-chip model provides a versatile platform not only for fundamental vascular research but also for screening new drugs and designing drug carriers. Several experiments were done to evaluate the model's reliability, and the results indicated high agreement with earlier models. The device's sensitivity towards antiplatelet drugs and targeted peptides suggests the potential use to test new drugs and drug carriers. Our device was purposely designed to allow the introduction of other plaque components such as macrophages, foam cells, smooth muscle cells, debris, lipids, and a variable amount of fibrous connective tissue for extended studies in future. These will be included in our next study together with the introduction of vascular endothelial cells and smooth muscle cells. Furthermore, our design will also allow studying the interaction of components in the blood vessel (main channel) and those in the plaques (supporting channel) thanks to the membrane (porous) structure at the stenosed area. We believe that the design would give an advantageous real-time platform to the researchers for studying the biomolecular interaction between atherosclerosis biomarkers and other elements. Altogether, we are aiming to develop a robust model to introduce complex plaque components with endothelial lining to mimic the physiological plaque microenvironment and develop our device as a more reliable alternative to in vivo models.

4. Limitations

The current design cannot generate a smooth hydrogel layer at the stenosis area, but the overall height of the hydrogel and thus the overall stenosis level are reproducible. Indeed, in blood vessels, the shape of the ruptured plaques varies, and their surfaces are not smooth. Therefore, our device mimics in vivo apparency of ruptured plaques.[71] Also, the current model used citrated blood to test the antiplatelet efficacy of aspirin. In vitro platelet function assays for testing the antiplatelet efficacy of the drugs are highly dependent on the type of *ex vivo* anticoagulant used during blood collection.[72,73] We may consider using different anticoagulants such as hirudin for blood collection and other known antiplatelet drugs such as P2Y12 receptor blockers to improve the model reliability as a drug testing device. Moreover, the model cannot develop a stable thrombus in the stenosis region and starts to dislodge after reaching the occlusion point. This attribute might be helpful in studying the effect of thrombus dislodgement in the bloodstream in future. Finally, we did not use cells or any complex plaque components, which could be considered another limitation of the current study.

5. Conclusion

We successfully developed and tested a site-specific atherothrombosis model on a microfluidic device for bridging the gap between in vitro and in vivo studies. This low-cost reusable device would provide a versatile platform for fundamental vascular research and expand the usage for discovering and testing drugs or drug carriers. We first optimized a standard technique for infusing thrombogenic substances into the supporting channel. We subsequently investigated the correlation between the vessel geometry and thrombus formation in our device to check the reliability of our design. The results showed that rapid platelet aggregation occurred on the device with higher stenosis. The thrombus size increased proportionally with time and occluded the main channel completely in the devices with 64% stenosis after ≈20 min of blood perfusion. On the other hand, complete occlusion of the channel was achieved after ≈30 min of blood perfusion in the device with 45% stenosis, while some small aggregates were noticed in 15% stenosed device. These results are in excellent agreement with in vivo thrombus formation phenomenon, which confirms the reliability of our device. We also validated the effectiveness of the device by investigating the shear-induced platelet aggregation in the device and it showed a significant increase in thrombus area with increased shear rates. Alongside, the devices were able to show different phenomenon in occlusive thrombus formation at various stenosis with the same peak shear rate. Our finding provides the evidence of in vivo relevance of our chip to understand the geometry dependent flow distribution and atherothrombus formation on the chip. Furthermore, the device was able to detect the antiplatelet efficacy of aspirin in a dose-dependent manner. The reduction of the thrombus size was almost double when the blood was treated with 100×10^{-6} M aspirin compared to the blood treated with 50×10^{-6} M of aspirin, demonstrating its indispensable advantages in evaluating and screening new drugs. Finally, we tested the binding affinity of the targeted and non-targeted PNPs on the thrombus for designing drug carriers. The targeted Cy5-RGD-PNPs exhibited strong affinity to bind to the thrombus immediately after perfusion and completely covered the surface of the thrombus after 10 min. Collectively, the in vitro results obtained by this novel device demonstrate a considerable in vivo relevance, encouraging further studies. Notably, the chips can be reused after washing, presenting them highly economical. We believe that the device would be utilized to explore biochemical interaction of numerous variables during thrombus formation.

6. Experimental Section

Device Fabrication: The chips were fabricated by the standard photolithography and PDMS soft lithography techniques.[74,75] Briefly, a silicon master mould was fabricated using the deep reactive ion etching

technique. Subsequently, the silicon surface was treated with salinization to form a thin layer of the hydrophobic self-assembling units. PDMS mixture was made with a base to curing agent ratio of 10:1 (Sylgard 184 Silicone Elastomer, Dow Corning, Midland, MI) and poured on the silicon master mould. The mixture was then degassed in a desiccator to remove the bubbles and cured for 2 h at 75 °C. After PDMS solidification, the PDMS slab with embedded channels was peeled off from the silicon master mould. Holes were punched with a 0.75 mm tip to make the inlets and outlets. Next, the PDMS slabs were washed with isopropyl alcohol and water, air-dried, and kept in the oven (75 °C) for 2 min for complete drying. After that, a clean glass slide and the PDMS device were treated in oxygen plasma (PDC-002, Harrick Plasma, Ossining, NY) for 1.5 min. Finally, the treated PDMS chips and the glass slide were bonded together. This process creates a tight seal between the PDMS chip and the glass slide.

Formation of Hydrogel Scaffold in the Supporting Channel—Infusion of 10 wt% Gelatin (GEL) Solution into the Supporting Channel: Due to the interconnection, polymer solutions leaked into the main channel during infusion through the supporting channel. Several approaches were applied to minimise the leakage of the polymer solution into the main channel. Table S1 provides a summary of the hydrogel scaffold formation protocol in the supporting channel. Devices were washed and reused after each experiment as described in supplemental material Section 4 (Figure S5, Supporting Information).

GEL solution (10 wt%) was prepared by dissolving gelatin powder in PBS (pH-7.4) in a water bath at 70 °C under gentle stirring for 2 h. First, tygon tubes were inserted into the inlet and the outlet hole of both main and supporting channels. To infuse GEL solution into the supporting channel, two syringe pumps (New Era Pump System, NE-1000) were used. The first syringe pump was concurrently delivered PBS into the main channel to block polymer diffusion, and the second syringe pump infused GEL solution into the supporting channel, Figure 3 PBS was infused continuously through the main channel at a flow rate of 20 µL min^{-1}. Subsequently, GEL solution (45 °C) was delivered through the tygon tube from the syringe at a flow rate of 90 µL min^{-1}. The flow rate was reduced to 20 µL min^{-1} before the GEL solution entered into the inlet of the supporting channel. After filling the supporting channel with the GEL solution completely, the second syringe pump was stopped. While at the same time, the flow rate of the first syringe pump was subsequently increased to 60 µL min^{-1} to wash the leaked GEL solution from the main channel. After washing excess GEL solution from the main channel, the device was placed on ice to trigger the hydrogel formation, while the PBS was running continuously through the main channel at the rate of 40 µL min^{-1} for 15 min. After hydrogel formation, the chip was observed under the microscope to check the homogenous hydrogel layer over the porous junction region. The chip was stored overnight at 4 °C before use.

Formation of Hydrogel Scaffold in the Supporting Channel—Infusion of Gelatin (10 wt%)-Collagen (0.02 wt%) (GEL-COL) Solution into the Supporting Channel: 10 wt% GEL solution was prepared for the GEL-COL composite following the aforementioned method. The GEL solution was cooled to 37 °C before adding collagen. Rat tail collagen-I (4 mg mL^{-1}) stock was added into the GEL solution to obtain the final concentration at 0.02 wt% and mixed vigorously using a magnetic stirrer at 400 rpm for 10 min. According to the manufacturer, collagen can denature at above 45 °C, so it is crucial to keep the temperature of the solution below that value. The infusion of the GEL-COL solution was followed by the standard GEL infusion protocol except the temperature of the solution. The GEL-COL solution was kept at 37 °C during infusion. After the successful infusion of the solution, the device was observed under a microscope to check the quality of the hydrogel layer over the porous region. The device was kept in the icebox for 20 min for hydrogel maturation. After 20 min of incubation in the ice box, the device was placed on ice and the main channel was washed with triton X-100 for 15 min at a flow rate of 20 µL min^{-1} from the inlet-outlet and repeated for another 15 min from the outlet-inlet. Finally, the main channel was washed by PBS for 5 min from the inlet-outlet and repeated for another 5 min from the outlet-inlet at the same rate to wash triton X-100 from the main channel. The device was subsequently stored overnight at 4 °C before blood infusion.

Computational Fluid Dynamics: The 3D geometries of the microfluidic chip with the corresponding stenosis section were developed in COMSOL. The computational models mimicked the geometry of the curved sidewall of the main channel of the microfluidic devices after hydrogel infusion. Blood as the input flow were defined as a fluid with a density of 1060 kg m^{-3} and dynamic viscosity of 0.003 Pa.s. Laminar flow physics was applied with no-slip boundary conditions at walls. One inlet and one outlet were selected for the models. Three different velocities were used to the inlet. The velocities were calculated based on the cross-sectional area of the inlet and the different flow rates of 5, 10, and 15 µL min^{-1}, corresponding to the base wall shear rate of 1000, 2000, and 3000 s^{-1}, respectively. Navier-Stokes equations for the incompressible fluid with no external forces (Equations (1) and (2)) were solved using a stationary study solver

$$\rho(\vec{u}\cdot\nabla)\vec{u} = -\nabla p + \mu\nabla^2\vec{u} \quad (1)$$

$$\nabla\cdot\vec{u} = 0 \quad (2)$$

where u represents the velocity vector, ρ the density, μ the dynamic viscosity, and p the pressure of the fluid.

Blood Collection and Blood Sample Preparation: Human fresh whole blood samples were used in all experiments. The blood was collected from a healthy volunteer by venipuncture in 3.2% sodium citrate tubes (BD Biosciences). The blood was collected according to the ethical consent of the University of Queensland and Griffith University Human Ethics Committees (approval numbers 2 015 001 037 and 2021/598). The blood was used within 1.5 h of collection in all experiments to obtain consistent results (unless specified otherwise). Before blood perfusion through the main channel, platelets were labeled with $DiOC_6$ (0.5 µg mL^{-1}) and incubated for 5 min at room temperature for fluorescence observation. The blood was then diluted with PBS (pH-7.4) at a 1:1 ratio.[76] Hemodilution with up to 50% saline maintained thromboelastographic indices and also had a very little effect on platelets.[76,77]

Blood Perfusion Assay for the Site-Specific Atherothrombosis Formation on-Chip: $DiOC_6$-labeled blood was infused for 30 min through the main channel of the devices with different stenosis using the withdrawal option of the syringe pump at a rate of 4.998 µL min^{-1}, which corresponds to the physiological arterial base wall shear rate of 1000 s^{-1}. The calculation was described in supporting information (Section S6). The blood was perfused through the chips prepared by GEL hydrogel or GEL-COL composite hydrogel in all stenosis. Brightfield and fluorescence images were taken at 200× magnification using an inverted microscope (CKX53, Olympus) mounted with a digital camera (DP74, Olympus). CellSens software Version 3.1 was used to compare the thrombus size and occlusion time in different stenosis at 5 min intervals. The same optic system recorded all images, otherwise mentioned. Data (n = 3) was analyzed by image processing software FiJi/ImageJ (Java 1.8.0_172).

Shear-Dependent Platelet Aggregation: $DiOC_6$-labeld blood was perfused through the chip with 15% stenosis and prepared by GEL-COL hydrogel. The blood was run through the main channel of the chips at a base wall shear rate of 2000 and 3000 s^{-1} separately to check the influence of shear rate in platelet aggregation.

Determining Antiplatelet Efficacy of Aspirin on the Chip: Aspirin was added to the $DiOC_6$-labeled whole blood and incubated at room temperature for 10 min before the assay.[36] Due to the short lifetime of aspirin in solution, aliquots were prepared immediately before addition to the sample by dissolving into DMSO and then diluted into PBS (pH-7.4).[37] The blood was infused through the main channel of the 64% stenosed device prepared with GEL-COL composite hydrogel in the supporting channel at a base wall shear rate of 1000 s^{-1} for 25 min by the withdrawal function of the syringe pump. Images were taken at 5 min intervals to detect the site-specific platelet adhesion and thrombus formation. Imaging and analyzing the images were carried out as above.

Targeted Binding of the Arg-Gly-Asp Peptide-Labeled Polymeric Nanoparticles to the Thrombus under Flow: A detailed procedure of preparing Cy5-RAD-PNPs was described in supplemental information (Section 6). The particles binding was done by following Ta et al.[67]

Briefly, the main channel was blocked with bovine serum albumin (BSA) (1 wt% in PBS pH-7.4) for 1 h at room temperature. The $DiOC_6$-labeled blood was infused through the main channel of the 64% stenosed chip with GEL-COL composite hydrogel at a base wall shear rate of 1000 s^{-1} for 15 min to obtain a site-specific thrombus formation on the chip. The main channel was then washed by perfusing PBS (pH-7.4) for 5 min at a shear rate of 5000 s^{-1} until no blood cells were observed. Next, Cy5-RGD-PNPs (500 μg mL^{-1}- in PBS pH-7.4 containing 0.5 wt% BSA) was perfused through the main channel for 10 min at a base wall shear rate of 1000 s^{-1} and binding of PNPs on thrombus was observed under microscope. Cy5-RAD (Arg-Ala-Asp) peptide-PNPs were used as negative control and ran by following the same procedures to check the nontargeted binding affinity of the PNPs on thrombus. Imaging and analyzing the images were carried out as above.

Statistical Analysis of Data: Data were presented as mean ± standard deviation (SD) of three independent experiments. One-way ANOVA was used to analyze the significant differences. A p value of ≤0.05 was considered significant. Graphs were plotted using GraphPad Prism 9.

Supporting Information

Supporting Information is available from the Wiley Online Library or from the author.

Acknowledgements

The authors acknowledge the support from National Health and Medical Research Council (HTT: APP1037310, APP1182347, APP2002827), Heart Foundation (HTT: 102761), Australian Research Council (ARC) Discovery Project (NTN, JZ: DP180100055), and ARC DECRA Fellowship (JZ: DE210100692). The microfluidic device was fabricated in Queensland Microtechnology Facility, part of the Queensland node-Griffith of the Australian National Fabrication Facility, a company established under the National Collaborative Research Infrastructure Strategy to provide nano and microfabrication facilities for Australia's researchers.

Open access publishing facilitated by Griffith University, as part of the Wiley - Griffith University agreement via the Council of Australian University Librarians.

Conflict of Interest

The authors declare no conflict of interest.

Data Availability Statement

The data that support the findings of this study are available from the corresponding author upon reasonable request.

Keywords

atherosclerosis, atherothrombosis, chips, microfluidic, plaques, platelets

Received: December 8, 2021
Revised: May 6, 2022
Published online:

[1] V. Mallika, B. Goswami, M. Rajappa, *Angiology* **2007**, *58*, 513.
[2] N. V. Menon, H. M. Tay, K. T. Pang, R. Dalan, S. C. Wong, X. Wang, K. H. H. Li, H. W. Hou, *APL Bioeng.* **2018**, *2*, 016103.
[3] K. S. Cunningham, A. I. Gotlieb, *Lab. Invest.* **2005**, *85*, 9.
[4] W. Zheng, R. Huang, B. Jiang, Y. Zhao, W. Zhang, X. Jiang, *Small* **2016**, *12*, 2022.
[5] P. K. Patibandla, A. J. Rogers, G. A. Giridharan, M. A. Pallero, J. E. Murphy-Ullrich, P. Sethu, *Anal. Chem.* **2014**, *86*, 10948.
[6] Y. Shin, S. Lim, J. Kim, J. S. Jeon, H. Yoo, B. Gweon, *Lab Chip* **2019**, *19*, 3664.
[7] M. Rafieian-Kopaei, M. Setorki, M. Doudi, A. Baradaran, H. Nasri, *Int. J. Prev. Med.* **2014**, *5*, 927.
[8] M. Thiriet, M. Delfour, A. Garon, *Vascular Stenosis: An Introduction*, Springer, Berlin **2015**.
[9] W. Insull, *Am. J. Med.* **2009**, *122*, S3.
[10] L. Badimon, G. Vilahur, *J. Intern. Med.* **2014**, *276*, 618.
[11] R. G. Mannino, D. R. Myers, B. Ahn, Y. Wang, R. Margo, H. Gole, A. S. Lin, R. E. Guldberg, D. P. Giddens, L. H. Timmins, W. A. Lam, *Sci. Rep.* **2015**, *5*, 12401.
[12] N. V. Menon, H. M. Tay, S. N. Wee, K. H. H. Li, H. W. Hou, *Lab Chip* **2017**, *17*, 2960.
[13] Q. Yang, Z. Xiao, X. Lv, T. Zhang, H. Liu, *Int. J. Bioprint.* **2021**, *7*, 370.
[14] P. Cui, S. Wang, *J. Pharm. Anal.* **2019**, *9*, 238.
[15] J. Wu, M. Dong, C. Rigatto, Y. Liu, F. Lin, *NPJ Digit. Med.* **2018**, *1*, 7.
[16] S. Kim, J. D. Jonghe, A. B. Kulesa, D. Feldman, T. Vatanen, R. P. Bhattacharyya, B. Berdy, J. Gomez, J. Nolan, S. Epstein, P. C. Blainey, *Nat. Commun.* **2017**, *8*, 13919.
[17] K. Hosokawa, T. Ohnishi, T. Kondo, M. Fukasawa, T. Koide, I. Maruyama, K. A. Tanaka, *J. Thromb. Haemostasis* **2011**, *9*, 2029.
[18] Y. Yamaguchi, T. Moriki, A. Igari, Y. Matsubara, T. Ohnishi, K. Hosokawa, M. Murata, *Thromb. Res.* **2013**, *132*, 263.
[19] N. Tsujii, K. Nogami, H. Yoshizawa, T. Sakai, K. Fukuda, A. Ishiguro, M. Shima, *J. Pediatr.* **2020**, *226*, 266.
[20] M. Yamazaki, T. Ohnishi, K. Hosokawa, K. Yamaguchi, T. Yoneyama, A. Kawashima, Y. Okada, K. Kitagawa, S. Uchiyama, *J. Thromb. Haemostasis* **2016**, *14*, 1788.
[21] Y. Arima, K. Kaikita, M. Ishii, M. Ito, D. Sueta, Y. Oimatsu, K. Sakamoto, K. Tsujita, S. Kojima, K. Nakagawa, S. Hokimoto, H. Ogawa, *J Thromb. Haemostasis* **2016**, *14*, 850.
[22] E. Westein, A. D. van der Meer, M. Kuijpers, J. Frimat, Berg, A. V. d., J. Heemskerk, *Proc. Natl. Acad. Sci. USA* **2013**, *110*, 1357.
[23] B. A. Herbig, X. Yu, S. L. Diamond, *Biomicrofluidics* **2018**, *12*, 042201.
[24] W. S. Nesbitt, E. Westein, F. J. Tovar-Lopez, E. Tolouei, A. Mitchell, J. Fu, J. Carberry, A. Fouras, S. P. Jackson, *Nat. Med.* **2009**, *15*, 665.
[25] M. Lui, E. E. Gardiner, J. F. Arthur, I. Pinar, W. M. Lee, K. Ryan, J. Carberry, R. K. Andrews, *Int. J. Mol. Sci.* **2019**, *20*, 2967.
[26] N. V. Menon, C. Su, K. T. Pang, Z. J. Phua, H. M. Tay, R. Dalan, X. Wang, K. H. H. Li, H. W. Hou, *Biofabrication* **2020**, *12*, 045009.
[27] A. Jain, A. Graveline, A. Waterhouse, A. Vernet, R. Flaumenhaft, D. E. Ingber, *Nat. Commun.* **2016**, *7*, 10176.
[28] A. Yazdani, H. Li, J. D. Humphrey, G. E. Karniadakis, *PLoS Comput. Biol.* **2017**, *13*, 1005291.
[29] Y. S. Zhang, F. Davoudi, P. Walch, A. Manbachi, X. Luo, V. Dell'Erba, A. K. Miri, H. Albadawi, A. Arneri, X. Li, X. Wang, M. R. Dokmeci, A. Khademhosseini, R. Oklu, *Lab Chip* **2016**, *16*, 4097.
[30] P. F. Costa, P. H. J. Albers, J. E. A. Linssen, H. H. T. Middelkamp, L. van der Hout, R. Passier, A. van den Berg, J. Malda, A. D. van der Meer, *Lab Chip* **2017**, *17*, 2785.
[31] M. Hardy, S. Lessire, S. Kasikci, J. Baudar, M. Guldenpfennig, A. Collard, J. M. Dogné, B. Chatelain, H. Jacqmin, T. Lecompte, F. Mullier, *J. Clin. Med.* **2020**, *9*, 2515.
[32] A. Dupuy, L. Hagimola, S. A. N. Mgaieth, C. B. Houlahan, R. E. Preketes-Tardiani, P. R. Coleman, F. H. Passam, *Diagnostics* **2021**, *11*, 203.
[33] T. Q. Nguyen, W. T. Park, *Sens. Actuators, B* **2020**, *321*, 128590.

[34] T. Hoefer, A. Rana, B. Niego, S. Jagdale, H. J. Albers, E. E. Gardiner, R. K. Andrews, A. D. van der Meer, C. E. Hagemeyer, E. Westein, *Haematologica* **2020**, *106*, 2874.
[35] J. Zilberman-Rudenko, J. L. Sylman, H. H. S. Lakshmanan, O. J. T. McCarty, J. Maddala, *Cell. Mol. Bioeng.* **2017**, *10*, 16.
[36] M. Li, N. A. Hotaling, D. N. Ku, C. R. Forest, *PLoS One* **2014**, *9*, 82493.
[37] K. Hosokawa, T. Ohnishi, M. Fukasawa, T. Kondo, H. Sameshima, T. Koide, K. A. Tanaka, I. Maruyama, *Microvasc. Res.* **2012**, *83*, 154.
[38] W. Z. Abdullah, S. A. Bakar, W. S. W. M. Zain, Z. Yusof, R. Mustaffa, R. Hassan, *Lab. Med.* **2013**, *44*, 90.
[39] C. Gachet, B. Aleil, *Eur. Heart J. Suppl.* **2008**, *10*, A28.
[40] M. Aziz, K. S. Yadav, *Med. Clin. Rev.* **2016**, *2*, 22.
[41] L. D. C. Casa, D. N. Ku, *Annu. Rev. Biomed. Eng.* **2017**, *19*, 415.
[42] I. Provenzale, S. L. N. Brouns, P. E. J. van der Meijden, F. Swieringa, J. W. M. Heemskerk, *Micromachines* **2019**, *10*, 787.
[43] S. M. Jung, M. Moroi, *J. Biol. Chem.* **1998**, *273*, 14827.
[44] R. W. Farndale, J. J. Sixma, M. J. Barnes, P. G. de Groot, *J. Thromb. Haemostasis* **2004**, *2*, 561.
[45] D. E. Roberts, A. McNicol, R. Bose, *J. Biol. Chem.* **2004**, *279*, 19421.
[46] I. Induruwa, M. Moroi, A. Bonna, J.-D. Malcor, J.-M. Howes, E. A. Warburton, R. W. Farndale, S. M. Jung, *J. Thromb. Haemostasis* **2018**, *16*, 389.
[47] L. Zhou, A. H. Schmaier, *Am. J. Clin. Pathol.* **2005**, *123*, 172.
[48] Y. Zhou, A. Yasumoto, C. Lei, C. J. Huang, H. Kobayashi, Y. Wu, S. Yan, C. W. Sun, Y. Yatomi, K. Goda, *eLife* **2020**, *9*, 52938.
[49] F. Akther, P. Little, Z. Li, N.-T. Nguyen, H. T. Ta, *RSC Adv.* **2020**, *10*, 43682.
[50] B. D. Walters, J. P. Stegemann, *Acta Biomater.* **2014**, *10*, 1488.
[51] M. A. Cejas, W. A. Kinney, C. Chen, J. G. Vinter, H. R. Almond, Jr., K. M. Balss, C. A. Maryanoff, U. Schmidt, M. Breslav, A. Mahan, E. Lacy, B. E. Maryanoff, *Proc. Natl. Acad. Sci. USA* **2008**, *105*, 8513.
[52] P. A. Evans, S. Heptinstall, E. C. Crowhurst, T. Davies, J. R. Glenn, W. Madira, S. J. Davidson, J. F. Burman, J. Hoskinson, C. M. Stray, *J. Thromb. Haemostasis* **2003**, *1*, 2140.
[53] U. Thaler, E. Deusch, S. A. Kozek-Langenecker, *Anaesthesia* **2005**, *60*, 554.
[54] A. J. Lusis, *Nature* **2000**, *407*, 233.
[55] L. Badimon, T. Padró, G. Vilahur, *Eur. Heart J. Acute Cardiovasc. Care* **2012**, *1*, 60.
[56] H. Buchwald, D. W. Hunter, N. Tuna, S. E. Williams, J. R. Boen, B. J. Hansen, J. L. Titus, C. T. Campos, *Atherosclerosis* **1998**, *138*, 391.
[57] D. Hackett, G. Davies, A. Maseri, *Eur. Heart J.* **1988**, *9*, 1317.
[58] D. M. Braganza, M. R. Bennett, *Postgrad. Med. J.* **2001**, *77*, 94.
[59] K. S. Sakariassen, L. Orning, V. T. Turitto, *Future Sci. OA* **2015**, *1*, FSO30.
[60] J. D. L. Bark, A. N. Para, D. N. Ku, *Biotechnol. Bioeng.* **2012**, *109*, 2642.
[61] H. T. Ta, N. P. Truong, A. K. Whittaker, T. P. Davis, K. Peter, *Expert Opin. Drug Delivery* **2018**, *15*, 33.
[62] A. Javadzadegan, A. S. C. Yong, M. Chang, A. C. C. Ng, J. Yiannikas, M. K. C. Ng, M. Behnia, L. Kritharides, *Am. J. Physiol.: Heart Circ. Physiol.* **2013**, *304*, H559.
[63] K. S. Sakariassen, R. Joss, R. Muggli, H. Kuhn, T. B. Tschopp, H. Sage, H. R. Baumgartner, *Arteriosclerosis* **1990**, *10*, 276.
[64] H. R. Baumgartner, K. S. Sakariassen, *Ann. N. Y. Acad. Sci.* **1985**, *454*, 162.
[65] T. D. Warner, S. Nylander, C. Whatling, *Br. J. Clin. Pharmacol.* **2011**, *72*, 619.
[66] Y. Liu, Q. Yang, H. Zhang, S. Han, N. Liu, H. Ren, H. Guo, F. Xu, *Drug Discovery Today* **2021**, *26*, 1875.
[67] H. T. Ta, S. Prabhu, E. Leitner, F. Jia, D. von Elverfeldt, K. E. Jackson, T. Heidt, A. K. N. Nair, H. Pearce, C. von zur Muhlen, X. Wang, K. Peter, C. E. Hagemeyer, *Circ. Res.* **2011**, *109*, 365.
[68] A. A. S. Rizvi, A. M. Saleh, *Saudi Pharm. J.* **2018**, *26*, 64.
[69] R. B. Basani, G. D'Andrea, N. Mitra, G. Vilaire, M. Richberg, M. A. Kowalska, J. S. Bennett, M. Poncz, *J. Biol. Chem.* **2001**, *276*, 13975.
[70] J. Sánchez-Cortés, M. Mrksich, *Chem. Biol.* **2009**, *16*, 990.
[71] R. B. Singh, S. A. Mengi, Y. J. Xu, A. S. Arneja, N. S. Dhalla, *Exp. Clin. Cardiol.* **2002**, *7*, 40.
[72] H. Z. Zhang, L. H. Yu, M. H. Kim, *Platelets* **2013**, *24*, 339.
[73] C. A. C. M. Pittens, H. J. Bouman, J. W. Van-Werkum, J. M. Ten-Berg, C. M. Hackeng, *J. Thromb. Haemostasis* **2009**, *7*, 1929.
[74] G. M. Whitesides, E. Ostuni, S. Takayama, X. Jiang, D. E. Ingber, *Annu. Rev. Biomed. Eng.* **2001**, *3*, 335.
[75] J. Zhang, N. Chintalaramulu, R. Vadivelu, H. An, D. Yuan, J. Jin, C. H. Ooi, I. E. Cock, W. Li, N.-T. Nguyen, *Anal. Chem.* **2020**, *92*, 11558.
[76] X. D. Manz, H. J. Albers, P. Symersky, J. Aman, A. D. van der Meer, H. J. Bogaard, R. Szulcek, *J. Visualized Exp.* **2020**, *159*, e61068.
[77] M. D. Tobias, D. Wambold, M. A. Pilla, F. Greer, *J. Clin. Anesth.* **1998**, *10*, 366.